

We are IntechOpen, the world's leading publisher of Open Access books Built by scientists, for scientists

6,900

Open access books available

186,000

International authors and editors

200M

Downloads

Our authors are among the

154

Countries delivered to

TOP 1%

most cited scientists

12.2%

Contributors from top 500 universities



WEB OF SCIENCE™

Selection of our books indexed in the Book Citation Index
in Web of Science™ Core Collection (BKCI)

Interested in publishing with us?
Contact book.department@intechopen.com

Numbers displayed above are based on latest data collected.
For more information visit www.intechopen.com



Fiber Sensor Applications in Dynamic Monitoring of Structures, Boundary Intrusion, Submarine and Optical Ground Wire Fibers

Xiaoyi Bao, Jesse Leeson, Jeff Snoddy and Liang Chen
University of Ottawa, (Physics Department)
Canada

1. Introduction

The pressure of reducing cost in industrial sectors has pushed the development of monitoring techniques for civil structures, transportation departments, manufacturing processes and security related applications. For the applications of civil engineering monitoring, we refer to bridges, tunnels, highways, railways, dams, pipelines, seaports and airports, which are associated to our daily lives. To assure them operating in good condition requires static and dynamic monitoring of strains and vibrations, which provides insight of the structural condition similar to monitoring human health. By identifying the abnormal vibration patterns via the frequency range and amplitude, or the strain magnitude and distribution, structural engineers can access the condition of civil structures. This may act as a warning sign for potential problems and to trigger the repairing process to prevent potential disaster and to protect our citizens. All useful monitoring tools should be able to find critical events via unusual frequency ranges and strain readings, which are stored as record for a specific structure for the purpose of determining the repairing time and scopes. Another front of important application is fiber cable monitoring, such as aerial, submarine and optical ground wire (OPGW) around high voltage power lines. The motivation of monitoring submarine and aerial fibers is to identify the fast polarization changes, as the polarization effect induces pulse broadening in dynamic fashion due to environmental effects, such as temperature and wind, and hence errors in the high speed communication system at rates higher than 10 GB/s. This monitoring process also produces an additional benefit: as the rotation of the polarization state is also proportional to the surrounding magnetic field via the Faraday effect. This means one can explore the high electrical current phenomena via polarization effect to identify local high magnetic fields, if the measurement is distributed, so that we can protect the power system.

The application to water wave and current measurement is driven by the advantage of fiber sensors with large coverage in environments such as seaports, rivers and waterways. Marine biologists use sound to identify marine mammals. Geophysicists record deep-sea seismic events from resulting pressure waves. The measured acoustic frequency varies for each application, with seismicity monitored at O(5 Hz), marine mammals at O(50 Hz) and ship passage at O(100 Hz). This frequency range is similar to the concrete bridge monitoring

requirement with much larger coverage than the bridges due to the size of the waves in water.

Although the above applications are very different, they are all related to the measurement of birefringence change in optical fibers. When the fiber is disturbed locally by stress, temperature or acoustic wave, the local birefringence will change. This change can be measured in the form of a polarized light change in transmission using direct detection or phase change by interferometers, and Rayleigh scattering or Brillouin gain for its dependence on the polarization state change.

2. Birefringence and Polarization Effects

When a monochromatic plane-wave (linear polarized beam) with a wavelength λ is launched in optical fibers, the electrical field can be described as

$$\vec{E}(\vec{r}) = E_x(z)\vec{i} \exp(-j\omega t) + E_y(z)\vec{j} \exp(-j\omega t) \quad (1)$$

where E_x and E_y are the electrical fields projection in the x and y directions at position z , $E_x(z) = E_{x0} \exp[j(\beta_x z + \delta_x)]$ and $E_y(z) = E_{y0} \exp[j(\beta_y z + \delta_y)]$, and $\beta_x = n_x k$ and $\beta_y = n_y k$ are the propagation constants, for the case of homogeneous and isotropic medium, $n_x = n_y = n_z$ and $k = 2\pi/\lambda$ which is the free space propagation constant, $\omega = 2\pi\nu$ is the angular frequency. The light is propagating in z -direction. The state of polarization (SOP) refers to the electrical field behavior at a particular point in space. δ_x and δ_y are the initial phases at $z = 0$ for the electrical field which are associated to the initial polarization state, and E_{x0} and E_{y0} are the initial amplitude of the electrical field at $z = 0$. As fiber is a birefringent medium, the index of refraction of n_x and n_y are different ($n_x \neq n_y$) which gives different propagation velocities, which makes the polarization state changes along the fiber. To a good approximation, the fundamental fiber mode is linearly polarized in the x or y direction depending on whether E_x or E_y dominates. In this case, a single mode fiber (SMF) is not a truly single mode; it in fact supports two modes of orthogonal polarizations. The two orthogonally polarized modes of a single mode fiber are degenerate ($n_x \approx n_y$) under ideal condition.

A strictly monochromatic plane of electromagnetic light means an infinitely long wave train which is completely polarized with zero spectral width, which is highly coherent. Any real physical source has a finite spectral width, for a laser with narrow linewidth $\Delta\nu$ ($\Delta\nu \ll \nu_0$), ν_0 is central frequency of the light source, we can call it quasi-monochromatic waves. A quasi-monochromatic signal can be the superposition of a large number of randomly timed statistically independent pulses with the same central frequency, which is partially polarized light.

There are three time scales to consider in the partially polarized quasi-monochromatic light for the fluctuations of the amplitude and phase of the electric field (Brosseau, 1998) $\tau_1 \equiv 1/\nu_0$ ($\sim 10^{-15}$ s), the period of quasi-monochromatic light, which is the time duration for the wave to go through a complete cycle; 2) $\tau_2 \equiv 1/\Delta\nu$ ($\sim 10^{-9} - 10^{-4}$ s), the time of coherence, which provides a measure of the time interval over which a field acts like a monochromatic wave; and 3) $\tau_3 \equiv t_{\text{det}}$ ($\sim 10^{-3}$ s), which is the response time of the detector. When $\tau > \tau_2$, the amplitude and phase of the electric field are considered as random functions of time, such as natural light; $\tau < \tau_2$, we can take the amplitude and phase as constants, partially

polarized light exhibiting both intensity and phase fluctuations. If $\tau \ll \tau_2$, the electric field can be treated as polarized light and it can be described as an ellipse whose size, eccentricity and orientation are randomly changed in time and its orthogonal components are mutually correlated. For a light source of well-stabilized laser, the coherence time τ_2 can be as small as 10^{-4} s, equivalent to a linewidth of ~ 10 kHz, such as the external-cavity-laser (ECL). For a He-Ne laser, the linewidth is 1.5 GHz, which corresponds to $\tau_2 = 10^{-9}$ s.

The polarization state of the output electrical field in optical fiber depends on the orientation of the electrical field relative to the refractive index axes of the birefringent medium, such as optical fiber. It can be described by the Jones matrix (Measures, 2001)

$$\vec{E}(z, t) = \text{Re} \begin{bmatrix} E_{xo}(z, t) \exp[j(\beta_x z - \omega t + \delta_x)] \\ E_{yo}(z, t) \exp[j(\beta_y z - \omega t + \delta_y)] \end{bmatrix} \quad (2)$$

If we take phase as $\phi(z, t) = \beta_x z - \omega t + \delta_x$ and differential phase as $\delta(z) = (\beta_y - \beta_x)z + \delta_y - \delta_x = (n_y - n_x)kz + \delta_y - \delta_x$, then Eq. (2) can be re-written as

$$\vec{E}(z, t) = \begin{bmatrix} E_{xo} \cos \phi(z, t) \\ E_{yo} \cos[\phi(z, t) + \delta(z)] \end{bmatrix} \quad (3)$$

For homogeneous and isotropic medium, such as glass, $\delta(z) = \delta = \delta_y - \delta_x$. The polarization angle is defined as $\theta(z, t) = \arctan(\text{Re}[E_y(z, t)/E_x(z, t)])$. Using Eq. (3) we have

$$\theta(z, t) = \arctan \left(\frac{E_{yo} \cos[\phi(z, t) + \delta(z)]}{E_{xo} \cos \phi(z, t)} \right) \quad (4)$$

To determine the state of polarization (SOP) we introduce $\gamma = E_{yo}/E_{xo}$, and then we can write

$$\tan(\theta(z, t)) = \gamma [\cos \delta(z) - \sin \delta(z) \tan(\phi(z, t))] \quad (5)$$

When the fiber is subjected to a local disturbance, such as stress or temperature, it leads to the change of modal birefringence $\delta n = |n_x - n_y|$, so the SOP will change accordingly following the Eq. (4) of $\theta(z, t)$.

For a linear polarized light at the input end of the fiber, this means $\delta(0) = \delta_y - \delta_x = m\pi$ and $\tan \theta(0) = \gamma \cos(m\pi) = (-1)^m \gamma$. At the output end of the fiber, the polarization state varies due to environmental effects, which induces modulation to the SOP so that $\beta_x(z) \neq \beta_y(z)$. Hence $\delta(z)$ varies with position which causes the output intensity to change with the time and position following the disturbance. Based on this principle we can detect fast changes in aerial (Waddy et al., 2005) and submarine fibers (Zhang et al., 2006) due to the wind, sun radiation and wave changes, as well as the electrical current changes in optical ground wire (OPGW) (Leeson et al., 2009) for the purpose of polarization mode dispersion (Chen et al., 2007) compensation in transmission direction. To get the spatial information, we can use the backscattering light, such as Rayleigh and Brillouin scattering light. By sending a pulsed light to optical fiber, we can detect the disturbance location via optical time domain reflectometry (OTDR) (Barnoski & Jensen, 1976).

3. Rayleigh and Brillouin Scattering in Fibers

Scattering in general arises from microscopic or macroscopic variations in density, composition or structure of a material through which light is passing. In a glass fiber, the random ordering of molecules and the presence of dopants cause localized variations in density (and therefore refractive index) that are small compared to the wavelengths of light that are used. These give rise to Rayleigh scattering which causes attenuation of the forward-propagating signal (and creation of a backward-propagating wave) that is proportional to λ^{-4} . Rayleigh scattering is a linear scattering process in that the scattered power is simply proportional to the incident power. Also, no energy is transferred to the glass in Rayleigh scattering; therefore there is no change in frequency of the scattered light. In an homogeneous and isotropic dielectric medium such as glass, the response of the medium to an electric field (\vec{E}) is described by the polarisation vector (\vec{P}_s) defined as

$$\vec{P}_s = \epsilon_0 \chi \vec{E} \quad (6)$$

where ϵ_0 is the vacuum dielectric constant and χ is the medium susceptibility. The scattering is induced by fluctuations $\Delta\epsilon$ of the medium dielectric constant ϵ . These fluctuations can then cause a small polarisation change $\delta\vec{P}_s$ such that the displacement vector \vec{D}_s of the scattered field can be expressed as a linear combination of the scattered (\vec{E}_s) and the input field (\vec{E}_p) (Landau & Lifchitz, 1969)

$$\vec{D}_s = \epsilon_0 \epsilon \vec{E}_s + \Delta\epsilon \vec{E}_p = \epsilon_0 \epsilon \vec{E}_s + \delta\vec{P}_s \quad (7)$$

The spatial (x, y, z) and temporal (t) dependence of the scattered wave must then be described by the perturbed wave equation

$$\nabla^2 \vec{E}_s - \left(\frac{n}{c_0} \right)^2 \frac{\partial^2 \vec{E}_s}{\partial t^2} = \mu_0 \frac{\partial^2 \delta\vec{P}_s}{\partial t^2} \quad (8)$$

where μ_0 is the magnetic permeability of vacuum, c_0 is the velocity of light in vacuum and n is the refractive index of the medium.

Rigorously, $\Delta\epsilon$ is a tensor even for an isotropic medium, which can be separated into three components: a scalar scattering, a symmetric scattering and an anti-symmetric scattering (Landau & Lifchitz, 1969; Boyd, 2003). Fluctuations of pressure, temperature, entropy and density, i.e. all thermodynamic fluctuations, are the origin of scalar scattering, and hence, at the origin of Brillouin and Rayleigh scattering. Mathematically, scalar scattering is given by the trace of the fluctuation tensor $\Delta\epsilon$. The variation of $\Delta\epsilon$ is induced by the thermodynamic quantities ρ and T (Boyd, 2003)

$$\Delta\epsilon = \left(\frac{\partial\epsilon}{\partial\rho} \right)_T \Delta\rho + \left(\frac{\partial\epsilon}{\partial T} \right)_\rho \Delta T \quad (9)$$

The second term can be neglected because density fluctuations affect the dielectric constant significantly more than temperature fluctuations (the error of not taking that term into account is 2%). We now expand the density fluctuations in terms of pressure (p) and entropy (s) fluctuations

$$\Delta\rho = \left(\frac{\partial\rho}{\partial p} \right)_s \Delta p + \left(\frac{\partial\rho}{\partial s} \right)_p \Delta s \quad (10)$$

The first term corresponds to adiabatic density fluctuations associated to acoustic waves, which is the origin of Brillouin scattering. The second term is an isobaric density fluctuation (which is entropy or temperature fluctuations) and leads to Rayleigh scattering associated to a diffusion process. If we neglect the entropy fluctuations the dielectric constant fluctuation via density can be expressed as

$$\Delta\epsilon = \left(\frac{\partial\epsilon}{\partial\rho} \right)_T \left(\frac{\partial\rho}{\partial p} \right)_s \Delta p = \frac{\gamma_e}{\rho_0} \left(\frac{\partial\rho}{\partial p} \right)_s \Delta p, \quad (11)$$

where the electrostrictive constant γ_e , is defined (Boyd, 2003) as

$$\gamma_e = \rho_0 \left(\frac{\partial\epsilon}{\partial\rho} \right)_T \quad (12)$$

ρ_0 is the average density of the material.

If we assume that the sound wave propagates along the fibre optical axis, then the density fluctuation propagates according to (Boyd, 2003)

$$\frac{\partial^2 \Delta\rho}{\partial t^2} - \Gamma' \frac{\partial^2}{\partial z^2} \left(\frac{\partial \Delta\rho}{\partial t} \right) - V_A^2 \frac{\partial^2 \Delta\rho}{\partial z^2} = 0 \quad (13)$$

where Γ' is the damping parameter and V_A the velocity of the acoustic wave.

Brillouin scattering is a relatively narrow-band process with a natural linewidth of roughly 30 MHz in standard single-mode fiber in the spontaneous regime. The frequency relationships among several different scattering processes are shown in Fig. 1 (not to scale), in particular the Brillouin Stokes and anti-Stokes components are separated from the Rayleigh peak by the Brillouin frequency ν_B .

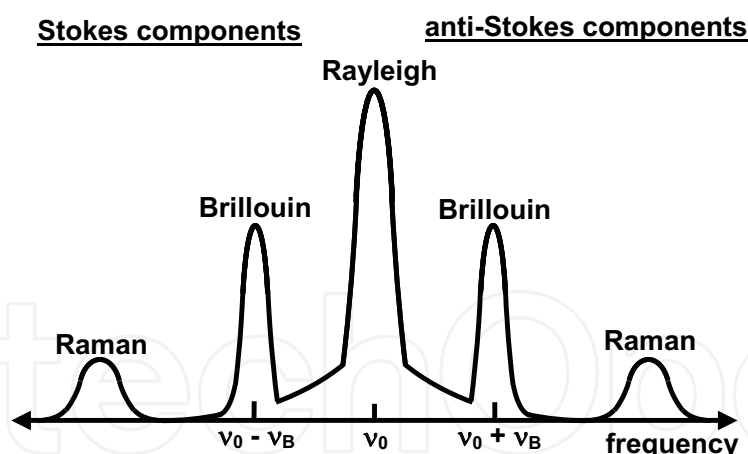


Fig. 1. Spontaneous scattering components (Snood, 2008).

4. Birefringence Effect in Submarine Fiber and Optical Ground Wire (OPGW)

With the development of higher speed communication system (> 10 GB/s), polarization mode dispersion (PMD) and polarization dependent loss (PDL) become additional limitations and a major source of concern for the system's performance (Huttner et al., 2000; Gordon & Kogelnik, 2000). It is important to measure the fastest PMD change, so that PMD compensation can follow the changes in real time.

The field test about the time evolution of polarization effects has been studied mostly in buried and aerial fibers. Previous experiments showed that in buried fibers, SOP drift is relatively slow, on the order of hours or days, and PMD fluctuation is due to temperature (Karlsson et al., 2000; Cameron et al., 1998; Allen et al., 2003); while in aerial fibers, SOP drift is relatively fast, on the order of microseconds in winter (Waddy et al., 2001), and PMD fluctuation is due to temperature, wind or even power line current variations since aerial fibers are often cabled together with power lines (Wuttke et al., 2003). Although, another type of fiber, submarine fiber, is widely used in global telecommunication networks, so far, very little work on polarization effects in it has been conducted, as submarine fibers are usually installed at remote areas, which are hard to get access to.

In May 2005, we had an opportunity to conduct a field test on three pairs of submarine fibers under Caribbean Sea, collaborated with Caribbean Crossing. One pair of fiber was measured ~ 26 hours with a fast PMD technique sampling at 15 s intervals. SOP information has usually been utilized to investigate the time evolution of polarization effects, which sets upper limit for PMD compensation in the high speed communications.

Since a fast polarization measurement was desired, the state-of-the-art polarization analyzer Adaptif A2000 was used for the test. Because we are interested in how fast the SOP and DGD decorrelate in submarine fibers (Zhang et al., 2006) we focused on the ACF (autocorrelation function) in the first few minutes. Fig. 2(a) describes the normalized ACF of SOP, PSP, DGD and cross correlation function (CCF) of SOP and PSP. There is some correlation between SOP and PSP within SOPs decorrelation time. Obviously, SOP decays faster than PSP and DGD. In Fig. 2(b) the decorrelation time was found to be 3 min for this combined submarine/buried fiber. The experimental ACF has a quick drop at the second point, which means the fastest change in this submarine fiber is less than 15 s. Fig. 2(c) compares the ACF of SOP during the day and night. The fitting parameter is chosen to be 1.1 and 5 min, respectively. As we expected, ACF in the day has a faster decay, which means the cable is in a relative static environment during the night. Similar to the wind effects on aerial fibers, the tension induced by ocean waves/currents may affect the signals in submarine fibers. Some segments may not touch the seabed but suspend over the trough, which is a normal situation for submarine fibers. It is natural to think the sun and moon are the main causes of the different current activities. The unevenness in ocean temperature, water density and salinity are the direct causes for currents. In the daytime, the solar radiation can strengthen these perturbations and hence, produce stronger currents. This may explain the different SOP drift times between the day and the night.

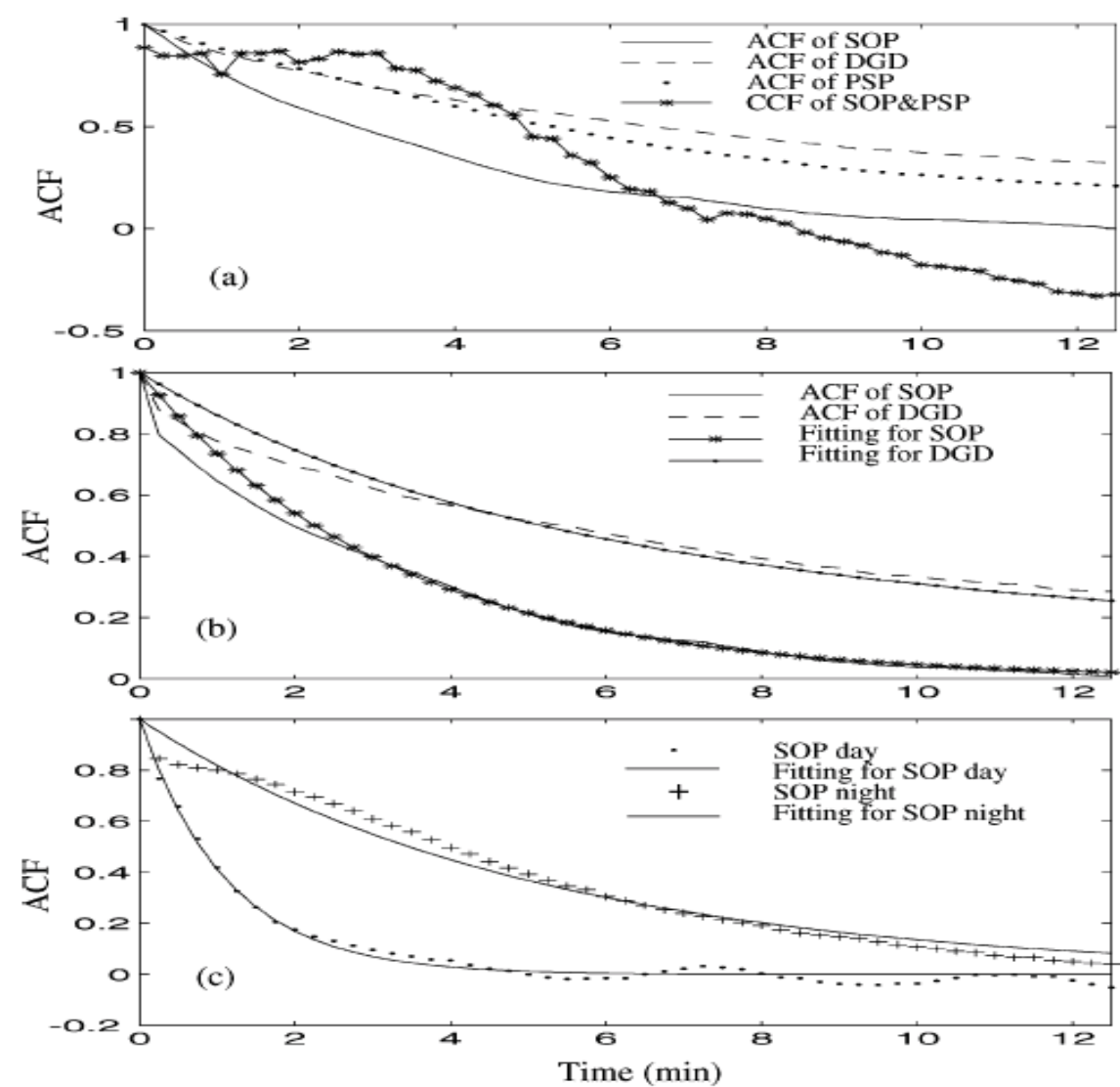


Fig. 2. (a) Small-scale view of experimental ACF of SOP, DGD, PSP, and CCF of SOP and PSP. (b) Comparison of theoretical and experimental ACF of SOP and DGD. (c) Comparison of experimental ACF of SOP during the day (11:00 A.M. to 18:00) and the night (23:00 to 6:00 A.M. the next morning) with corresponding curve fittings. From Zhang et al. (2006).

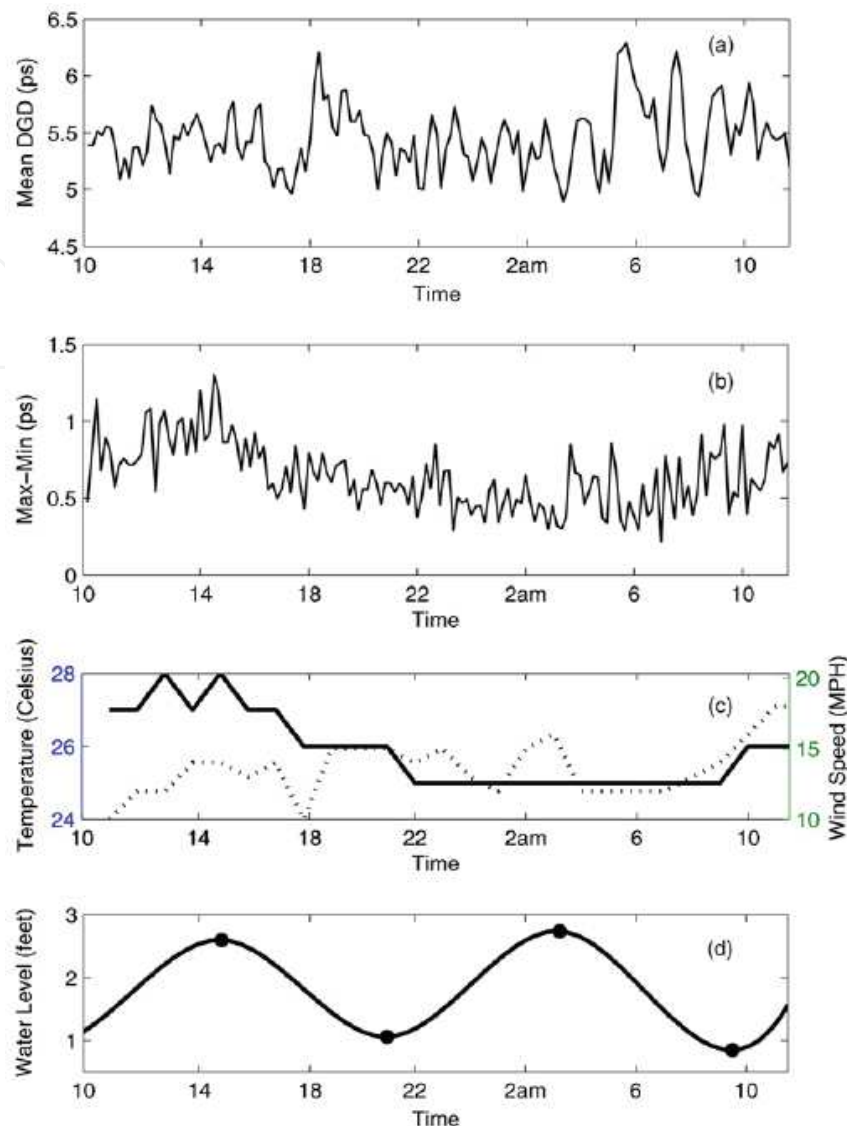


Fig. 3. (a) Time evolution of DGD averaged over both wavelength and 10 min time, (b) wavelength-averaged DGD fluctuation in every 10 min of fiber A, (c) temperature (solid line) and wind (dotted line) data during measurement period, (d) tide (vertical water level) information. From Zhang et al. (2007).

The time evolution of DGD averaged over wavelength at each 10 min interval is shown in Fig. 3(a). The PMD (mean DGD) over 26 h was calculated to be 5.45 ps. It was found in (Gisin et al., 1996) that with mean PMD $\langle \Delta\tau \rangle$ over wavelength range $\Delta\omega$, the uncertainty is $\Delta\tau \times 0.9 / \sqrt{\Delta\tau \times \Delta\omega}$. Using this relation, the uncertainty of the measurement was 0.27 ps. In order to investigate the PMD fluctuation within every 10 min, Fig. 3(b) shows the difference between maximum and minimum PMD value (mean DGD). The fluctuation is relatively large during the day and relatively small during the night, then it increases again in the following morning. We may conclude sun radiation is correlated to PMD fluctuation in submarine fibers. Fig. 3(d) shows the water level of the sea during the measurement period at one end of FUT. Two PMD peaks are observed in Fig. 3(a) at 18:20 in the first day and 6:00

am the next morning. They have some correlation to the large downward changes in tide level.

The time evolution of PMD is of greater interest to system designers. Tide is the periodic rise and fall of a body of water resulting from gravitational interactions between the Sun, Moon and Earth. It is the observed recurrence of high and low water along the seashore—usually, but not always, twice daily. Current associated with tide, is the horizontal flow of water. It floods in which makes the tide rise and ebbs out which makes the tide falls. As described in Fig. 3(d), the testing place has a semidiurnal tide, which means there are two high tides and two low tides in one day. The current may flow quickly when a high tide recedes. One high tide appeared at 15:00 and the subsequent low tide arrived at 21:00, so the current with maximum speed was around 18:00. Similarly the current flows quickly at about 6:15 next morning. Since the tidal/current effect has particular direction, at the moment of maximum current, submarine fiber should have the maximum induced tension or displacement if any, which corresponds to the large absolute PMD value. Therefore, around those two time moments, PMD reached two peak values as shown in Fig. 3(a). Since the distance between the two ends of fiber is about 80 km, it is conceivable that tide times at the two ends are different. And the fluctuation of PMD magnitude is a combined tidal effect on the cable over the entire length. Therefore, there are some smaller peaks following the main peaks in Fig. 3(a).

OPGWs are a common type of aerial fiber installed worldwide on high voltage power lines. An OPGW cable provides ground wire protection for important electrical current carrying power lines and a high capacity communication network. Due to the proximity of the OPGW to the electrical current there is magnetic field exposure to optical fiber in OPGW. The component of magnetic field in the propagation direction of the light signal induces circular birefringence by way of the first order Faraday effect, the resulting SOP dynamics are unique from typical aerial fiber (Leeson et al., 2009). The OPGW network provides new difficulties for PMD compensation designers because polarization changes can reach 300 Hz due to harmonic magnetic fields. On the other hand, the magnetic field exposure may allow high magnetic field detection providing SHM from ice buildup on ground wires and power lines, a major problem during the winter in many areas where high voltage power lines are deployed.

In August 2007, we conducted a field test on two different fibers installed within an OPGW. The measurement was ~ 60 hours. The SOP changes were monitored simultaneously on both fibers using two Agilent 8509 polarization analyzers at a sampling rate of 1 KHz. A major difficulty in the development of a polarization monitoring technique for SHM of the OPGW network is the presence of time varying birefringence from temperature changes, wind (Aeolian vibrations/cable swings) and solar radiation. The drift of polarization entering a magnetic field section de-correlates the linear relation between magnetic field and the SOP changes. A Faraday Rotating Mirror (FRM) should be installed to observe the nature of the magnetic field induced birefringence, as it minimizes static and quasi-static reciprocal birefringence. For this reason, we monitored two fibers, one fiber's transmission and another with an FRM installed, Fig. 4 shows the power spectrum up to 330 Hz calculated for a one min daytime period for both fibers. In Fig. 4(a), on this time scale for the transmission signal, we observe a peak at < 1 Hz, a large spectral base up to ~100 Hz and a 60 Hz peak with 120 Hz and 180 Hz harmonics. The < 1 Hz peak is correlated to OPGW cable swings as discussed in (Wuttke et al., 2003). The 0 Hz to ~100 Hz spectral base matches

the OPGW the natural Aeolian frequency of 10 - 80 Hz for a wind speed range of 3.6 to 25.2 km/h (Krispin et al., 2007). Because we observe very similar frequencies to the reported natural Aeolian frequencies, and the wind is 17 km/h during this period, these modulations are most likely due to this environmental effect. The 60 Hz peak exists because the electrical current carried by the high voltage lines is 60 Hz and is modulating the SOP by the Faraday effect; the harmonic peaks exist due to nonlinear voltage/electrical current properties of electrical devices that result in harmonic magnetic fields each modulating the SOP. In Fig. 4(b) we see the effect the FRM has on improving our observation of the nature of the magnetic field induced SOP changes. We observe the same 60 Hz peak resulting from the 60 Hz electrical current and now harmonic peaks up to 300 Hz. 300 Hz is the fastest polarization modulation reported in OPGW/aerial fiber, this sets the requirement for PMD compensation on the OPGW network.

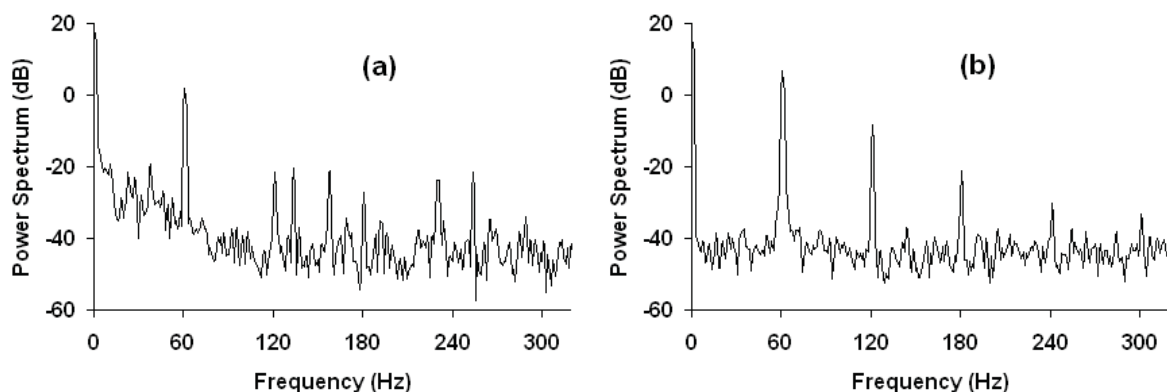


Fig 4. Power spectrum up to 330Hz calculated for a one minute daytime period (a) for transmission and (b) with an FRM installed. From Leeson et al. (2009)

We calculated for the OPGW fiber with the FRM installed the maximum arc length that is mapped out over a given time interval on the Poincare's sphere in radians, for PMD compensation information. The fast 60 Hz polarization changes are maximized for a time interval of 8 ms, for our sampling rate of 1 KHz. To observe the decorrelation over the entire measurement time we used the ACF of the SOP and defined t_{half} , which describes the time at which the SOP has de-correlated 50 % (Waddy et al., 2005). The change in the way the SOP de-correlates for 10 min intervals ($T = 600$ s) can then be observed using:

$$ACF50\%(t_{half}) = \frac{T - t_{half}}{T} \quad (14)$$

Where at the maximum value of $ACF50\% = 1$ there is the fastest SOP change possible. Fig. 5(a) shows data representing the fast surrounding SOP modulating phenomena, i.e. the wind speed and the electrical current carried by the neighboring conductors and Fig. 5(b) shows the maximum arc length in radians for one min periods and the $ACF50\%$. We see a correlation between the maximum arc length and the electrical current during the nighttime periods we could not observe without the FRM installed. The minimizing of temperature fluctuation and wind induced linear birefringence allows us to observe the magnetic fields contribution to polarization changes. As the FRM is not ideal, we still observe linear birefringence effects during the daytime period. During the daytime fast variations in the arc length appear. These variations must be caused by sun radiation induced temperature

gradients between the cable core and cable surface, because the variations show no apparent correlation to any other environmental factors. The ACF50% shows that SOP drift is correlated to electrical current during most of the acquisition time. The SOP Autocorrelation function is shown to de-correlate as electrical current increases despite the presence of the solar gradient effect during the day. It is therefore possible that electrical current may induce detrimental errors in high speed communication systems (> 10 Gb/s). While we have shown that the FRM is required for accurately detecting the electrical current, to provide location information a distributed Polarization-OTDR (POTDR) may be required with the FRM to locate and diagnose a disturbance.

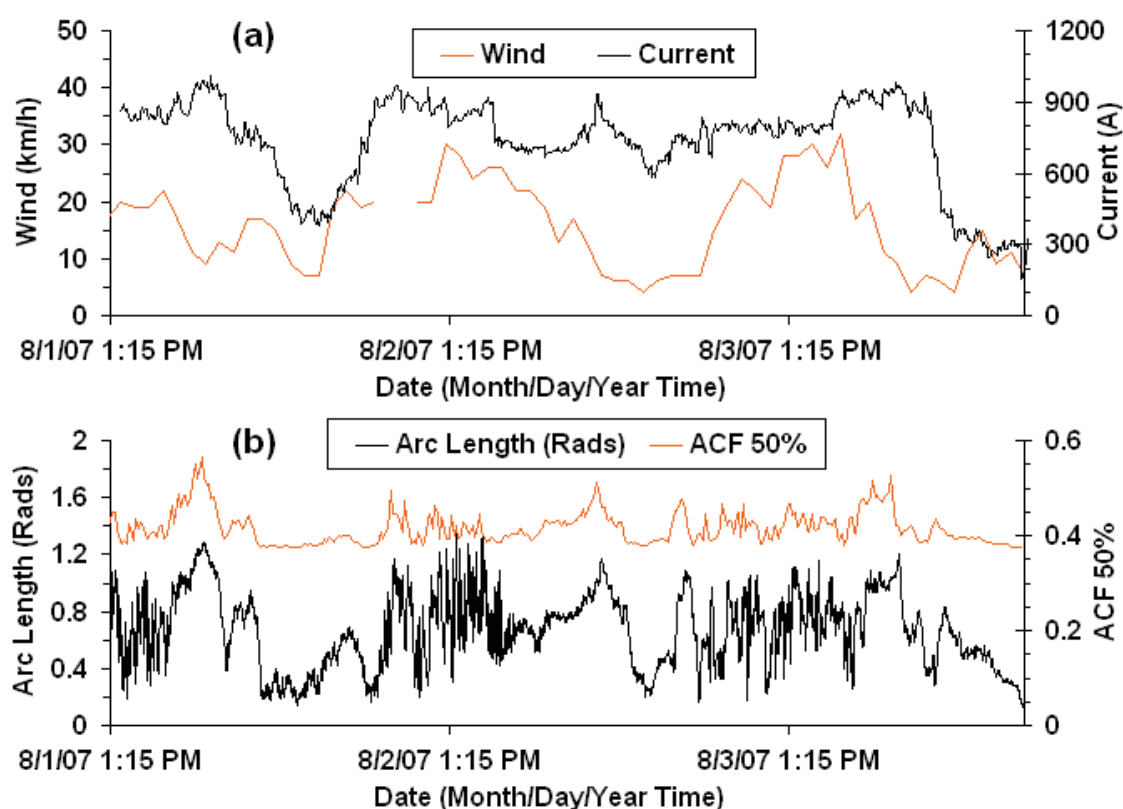


Fig. 5. (a) Wind and electrical current data plotted in an OPGW with a FRM installed and (b) calculated maximum arc length plotted with ACF 50%. From Leeson et al. (2009)

5. Distributed Fiber Vibration Sensor Based on Polarization Dependence in Stimulated Brillouin Scattering

5.1 The polarization dependence of the Brillouin gain

The distributed Brillouin sensor is an optical fiber based sensor that relies on the effect known as Brillouin scattering in order to measure the temperature and strain in a distributed fashion. The system monitors the interaction of two counter-propagating light waves within a sensing fiber by the pump and the probe waves. The Brillouin interaction results in power being transferred from the pump wave into the probe wave, and the efficiency of this process depends on several factors including the beat frequency between the pump and probe lasers, and the polarization states of these waves. The interaction is

optimized if the beat between the lasers matches the Brillouin frequency (probe wave at the Stokes frequency), which is a material property of the optical fiber, and if the polarization states are the same for pump and probe waves. The Brillouin frequency shift is linearly dependent on the temperature and strain of the fiber, allowing the system to measure both of these properties. The Brillouin frequency can be measured by sweeping the beat frequency of the pump and probe lasers over a range and measuring the loss of the pump wave (or gain of the probe wave) at each frequency to construct the Brillouin spectrum at each location in the sensing fiber. Spatial information is acquired by matching the time of flight of the pulse to a location in the fiber, a process known as Brillouin optical time domain analysis (BOTDA).

The vibration sensor based on stimulated Brillouin scattering is shown in Fig. 6. The probe wave gets amplified by the Brillouin interaction with the pump and it is this signal that is directed to the detection arm and measured (alternatively, the loss of the pump wave can be detected in the Brillouin loss technique). For optimal sensitivity, the pump and probe laser frequencies must be locked to the Brillouin frequency corresponding to the static strain of the optical fiber under test. At the fixed Brillouin frequency, one can measure the birefringence change induced modulation to the Brillouin gain spectrum as illustrated in Fig. 7.

There are two physical mechanisms that make it possible to detect vibrations of an optical fiber via the stimulated Brillouin scattering. One mechanism is the fact that as the fiber is undergoing vibration, there will be strain introduced along the fiber. The strain in the fiber will cause the Brillouin frequency of single mode fiber to shift by roughly $0.05 \text{ MHz}/\mu\epsilon$. This kind of measurement requires a polarization scrambler for each scanned Brillouin frequency.

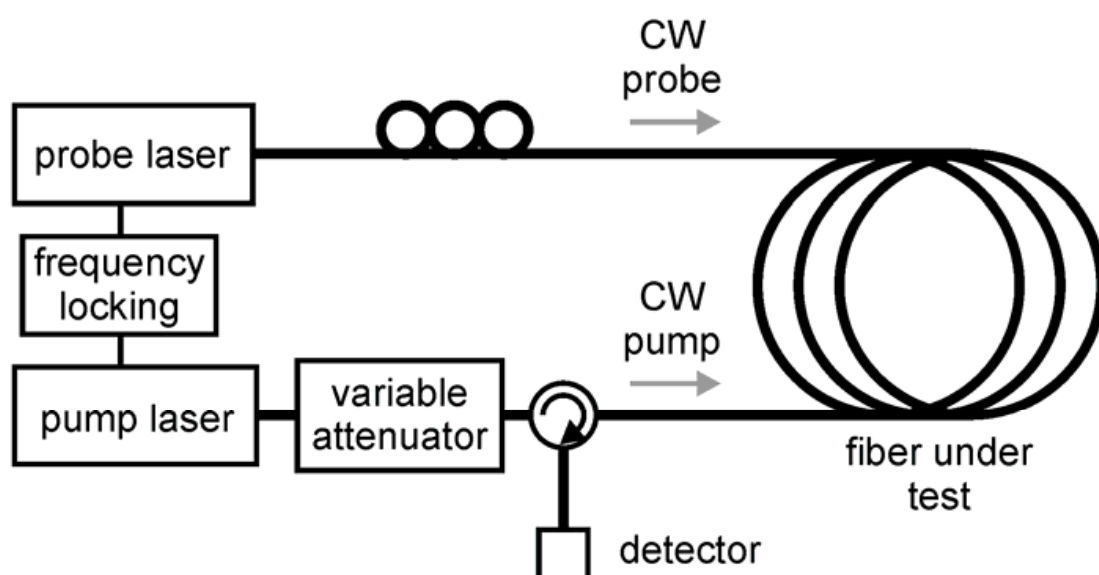


Fig. 6. Brillouin vibration sensor setup

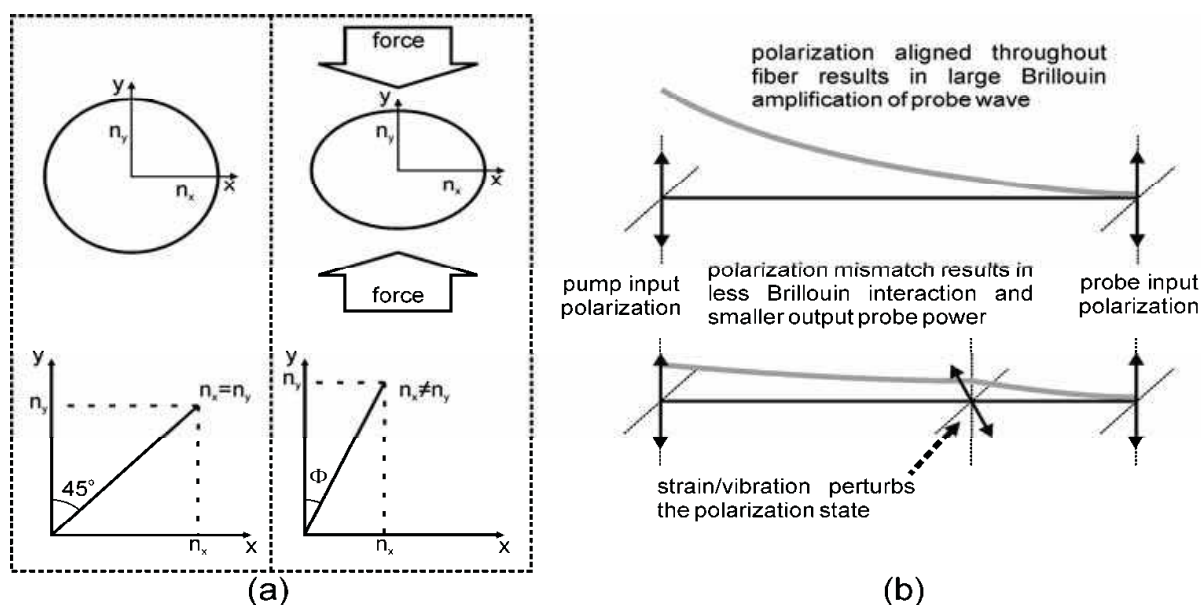


Fig. 7. (a) Local birefringence change caused by force on optical fiber. (b) Sensing mechanism based on perturbation of the polarization states – the growth in the probe wave traveling from right to left is represented by the thick black line. From Snoody (2008).

If the pump and probe polarization states are aligned for an unstrained loose fiber, the Brillouin interaction will be large throughout the entire fiber (the polarization states drift only gradually in the time scale of minutes as explained in section 4). When the fiber is disturbed, the Brillouin interaction will not be optimal and the detected probe power exiting the fiber will be reduced as depicted in Fig. 7(b).

To show the vibration induced birefringence change and the associated Brillouin gain change, the fiber under test was a 15 m length of standard single mode fiber wrapped around a piezo fiber stretcher vibrating at 100 Hz. The results in Fig. 8(a) show that the sensitivity of the system was improved by an order of magnitude due to the Brillouin amplification when the pump wave was turned on.

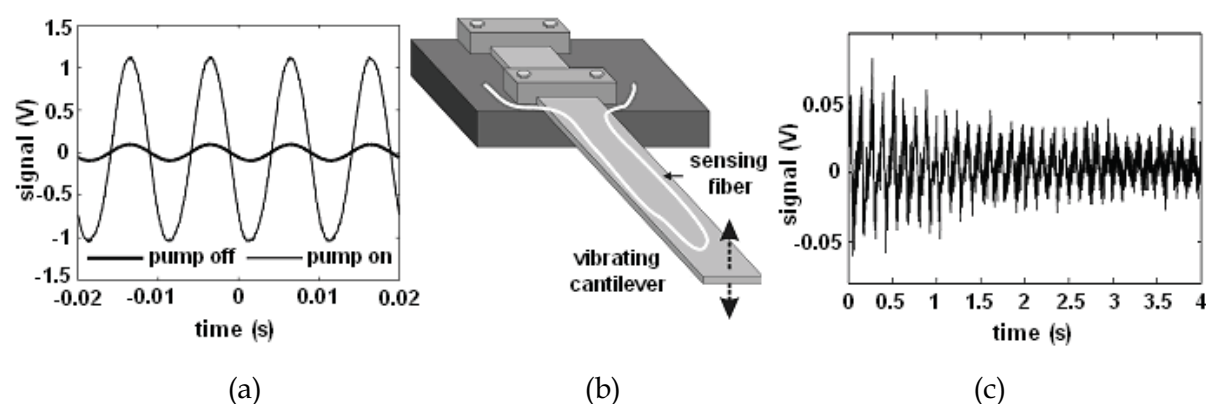


Fig. 8. (a) Effect of introducing pump wave – system sensitivity increases by an order of magnitude; (b) Experimental setup for vibrating cantilever; and (c) Experimental results for vibrating cantilever.

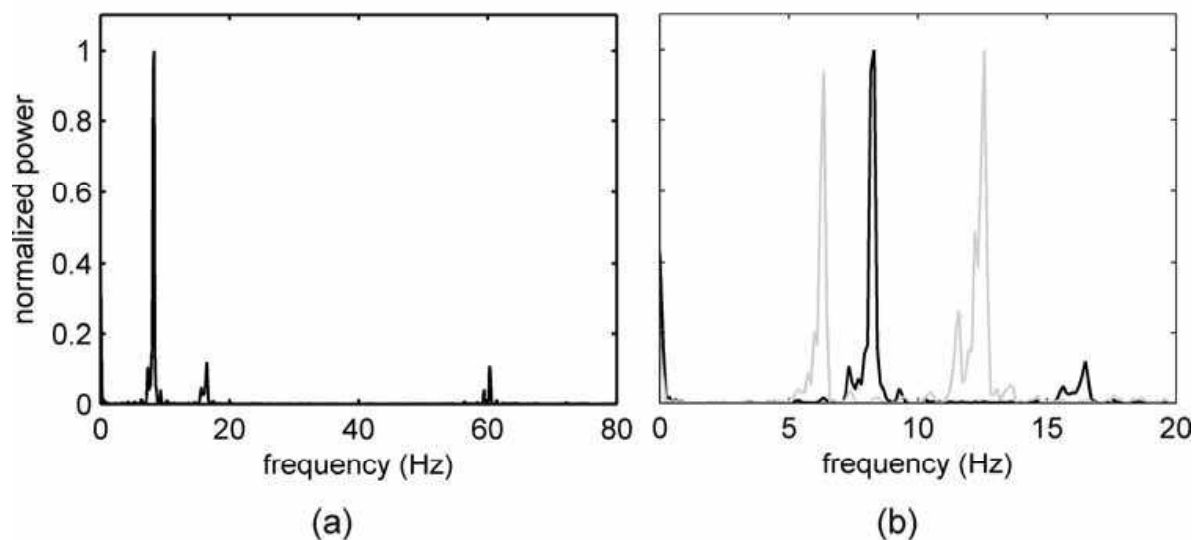


Fig. 9. (a) Power spectrum of vibrating cantilever; (b) Effect of damaging cantilever (grey)

The following experiment was done to detect the frequency of a vibrating steel cantilever. A section of fiber was bonded to the surface of a steel cantilever of which roughly 0.5 m was allowed to oscillate (Fig. 8(b)). The oscillations of the steel strip were clearly observed as well as the damping behavior of the vibration as seen in Fig. 8(c). Damage to structures can be detected by changes in vibration behavior, both amplitude and frequency, and so it is imperative to measure the frequency characteristics of the vibrating structure. The Fourier transform of the data of Fig. 8(c) was taken and the resulting power spectrum is shown in Fig. 9. The main vibration frequency of 8.5 Hz is clearly evident as well as smaller contributions at other frequencies including a peak at 60 Hz which is due to electrical mains noise and should be filtered out.

To test the system's capability to measure damage to a structure, the steel cantilever was damaged by adding a C-clamp to the beam and monitored. By observing the changes in the frequency spectrum, it is possible to see that the vibration characteristics of the cantilever have been modified, indicating structural damage. In Fig. 9(b), it can be seen that when damage was introduced the vibration frequencies shift lower and the relative power of the secondary peak has grown significantly.

5.2 Distributed vibration sensor based on birefringence of the Brillouin gain

To add distributed sensor ability we used 20 ns pulses equivalent to 2 m spatial resolution from a light source. With the pulsed probe wave, the Brillouin interaction only occurs at a particular fiber location when the pulse is present at that location. An 80 cm section of a 120 m fiber was bonded to a 40 cm steel cantilever which was allowed to vibrate. Fig. 10 shows the performance of the vibration sensor zoomed in on the fiber location which is vibrating. The data shown is the Brillouin loss signal which has been processed by subtracting the waveform for the stationary cantilever to reveal only the changes in the Brillouin signal as the cantilever vibrates. During the vibration the birefringence of the optical fiber is altered which perturbs the states of polarization of the pump and probe waves in that section of fiber. Since the strength of the Brillouin interaction depends on the alignment of the pump and probe SOP, this perturbation alters the strength of the Brillouin loss detected at the

vibrating location. The spatial resolution of the sensor is shown to be 2 m in Fig. 10(a), as expected for a 20 ns pulse. The small section of vibrating fiber is clearly visible against the background signal of the otherwise stationary fiber. Fig. 10(b) shows the vibration response of the steel cantilever as measured by the sensor at a single fiber position corresponding to the peak of the vibration response from Fig. 10(a) for 1 s at a sampling rate of over 100 Hz with each waveform consisting of 50 averages. The frequency of vibration of the cantilever is found to be 13 Hz.

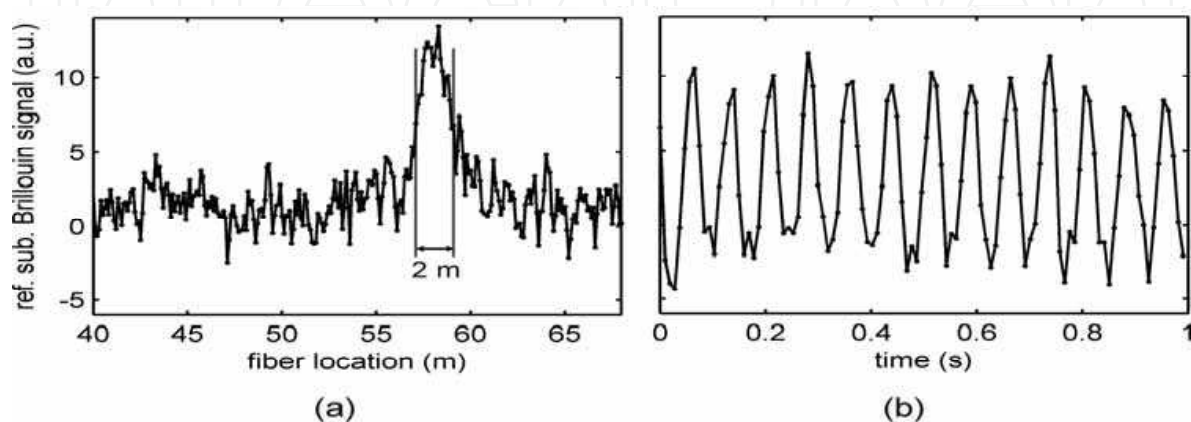


Fig. 10. (a) Spatial resolution of vibration sensor. (b) Vibration response of steel cantilever.

The distributed impact waves due to highway traffic on concrete slabs reinforced with fiber reinforced polymer (FRP) bars are monitored in real time using stimulated Brillouin scattering (Bao et al., 2008). The impact wave is caused by the traffic passing on the highway pavement at high speed (> 100 km/h), which induced pressure on the concrete slabs, and in turn created a local birefringence change, leading to variation of the local state of polarization change (SOP). The pump and probe waves of the stimulated Brillouin scattering 'see' the SOP change and react with a decrease of the Brillouin gain or loss signal relative to the input SOP of the pump and probe waves. The frequency difference between the pump and probe waves are locked at the static-strain-related Brillouin frequency. Optical fiber was embedded throughout the concrete pavement continuously reinforced with FRP bars in highway to detect impact waves caused by cars and trucks passing on these pavements at a sampling rate of 10 kHz. A spatial resolution of 2 m was used over a sensing length of 300 m. The maximum measured frequency was 15 Hz.

6. Measurement of the Vibration and Acoustic Wave in Structures

As explained in section 2, in single mode fiber the random imperfections during the manufacturing process breaks the circular symmetry of the fiber core, causing two orthogonally polarized components of light to travel with different velocities. The birefringence in fiber varies with many physical parameters such as: strain, temperature, pressure wave, ultrasonic fields, etc., leading to changes in the phase shift between two polarization eigenmodes. Thus, the output state of polarization (SOP) changes at the fiber end. By monitoring the power change of polarized light in the time and frequency domain, one can detect the impact wave as well as the vibration frequency in real time. This method has been used to characterize a PZT for its frequency response and phase delay (Zhang &

Bao, 2008a). The experimental setup is shown in Fig. 11. To test its impact wave response, a cantilever beam was designed with a piece of spring steel with dimension 320×40×0.9 mm (L×W×H), and one end was clamped on a stage. Its shape was designed to be an isosceles trapezoid, which experiences a uniform strength impact wave along the beam. The bare fiber (SMF-28) was taped by clear lightweight scotch tape on the beam with a total length of 60 cm. Impact wave was induced by the tip of a bent nose pliers at the fixed end. A slight tapping on the cantilever beam is applied to minimize the overall oscillations.

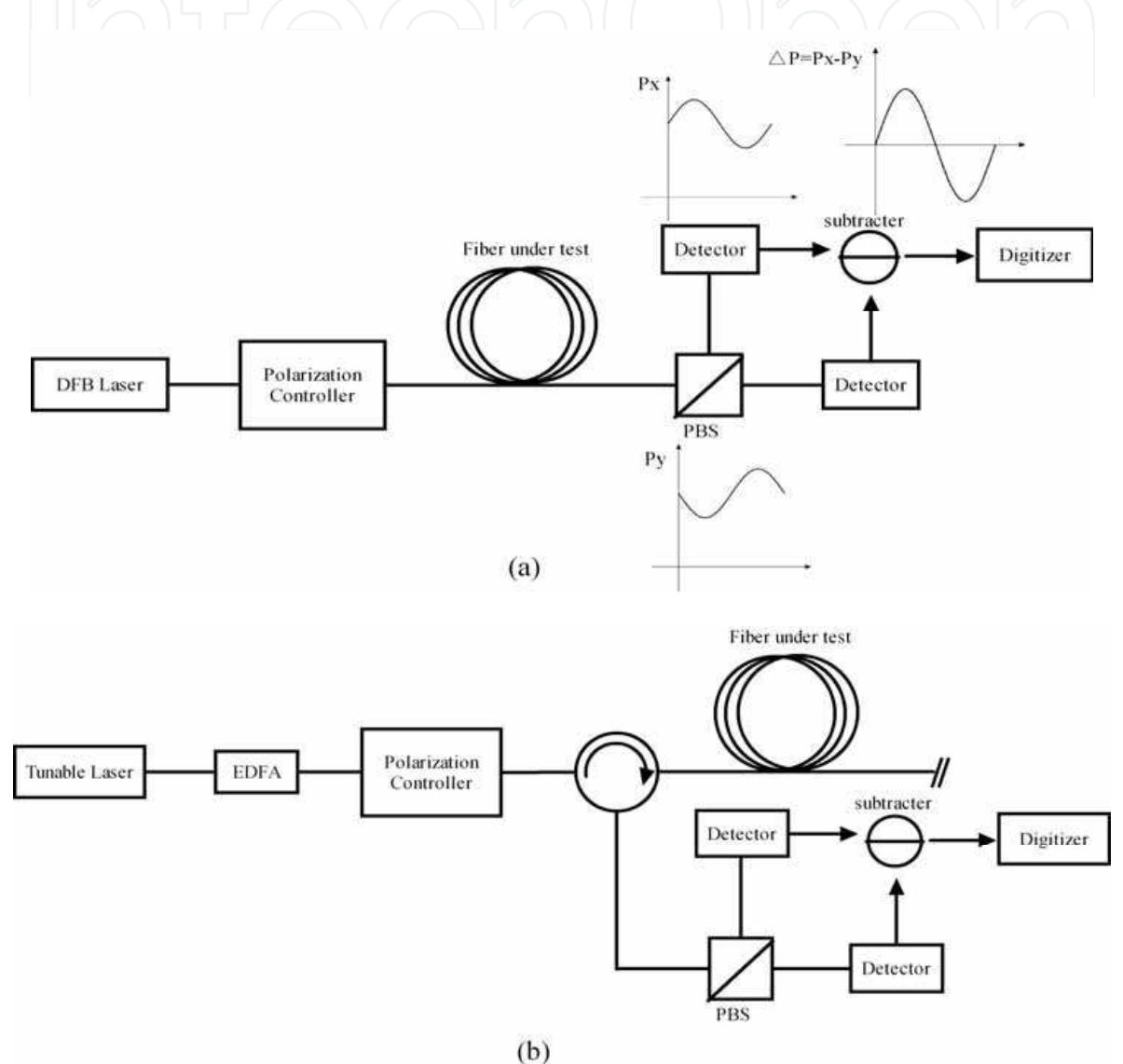


Fig. 11. Experimental setup of optical fiber diversity vibration/acoustic sensor for the transmission and Rayleigh backscattering.

Fig. 12(a) shows the response of the optical fiber sensor and an accelerometer after a single hit, both of which have clear damped trends in time domain. The result is obtained with no averaging or filtering (Zhang, 2008a). After the first 0.2 s, the accelerometer decays

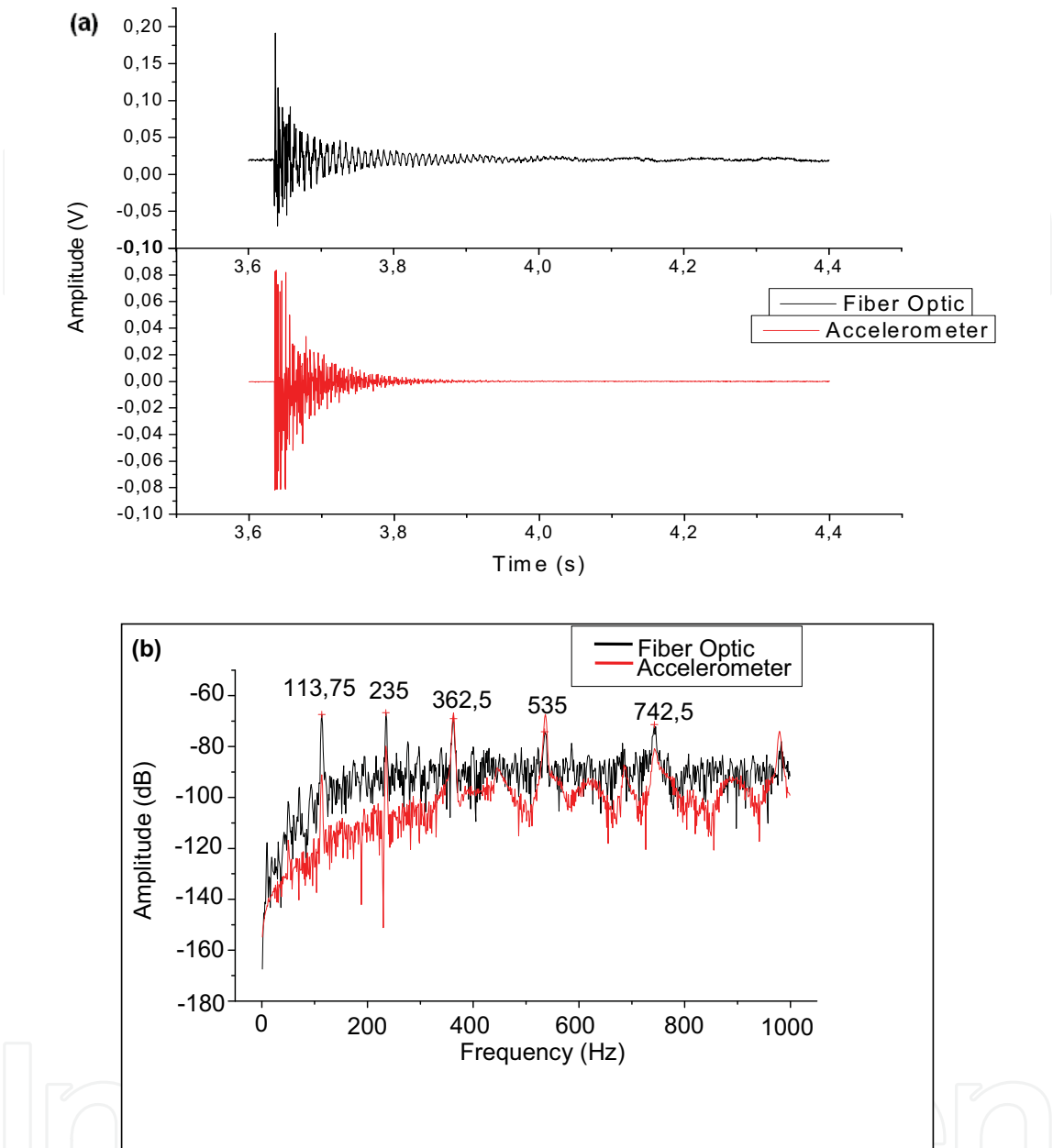


Fig. 12. Impact detection of a cantilever beam with the optical fiber sensor (black) and the accelerometer (red): (a) time trace; (b) normalized power spectrum (Zhang et al., 2008a)

to zero. While the optical fiber sensor still shows some small oscillations due to its long length coverage over the entire beam. In order to compare their frequency components, fast Fourier transforms are computed and the power spectrums are depicted in Fig. 12(b). All five main peaks appear at the same frequencies: 113.75 Hz, 235 Hz, 362.5 Hz, 535 Hz and 742.5 Hz, respectively, which represent different excited modes within the cantilever beam because of the strength of the initial hit. We also notice the tendency that the power spectrum amplitude of the accelerometer is lower than that of the fiber sensor. This is caused by a lower sensitivity of the accelerometer in the low frequency range. The

accelerator is designed to detect higher frequency components above a few hundred Hz. For low frequency vibration/acoustic measurements, velocity or displacement transducers work more efficiently than accelerometers. Apparently, the fiber sensor has the ability to detect wider frequency ranges to accurately measure the dynamic properties of structures under impact waves in real time.

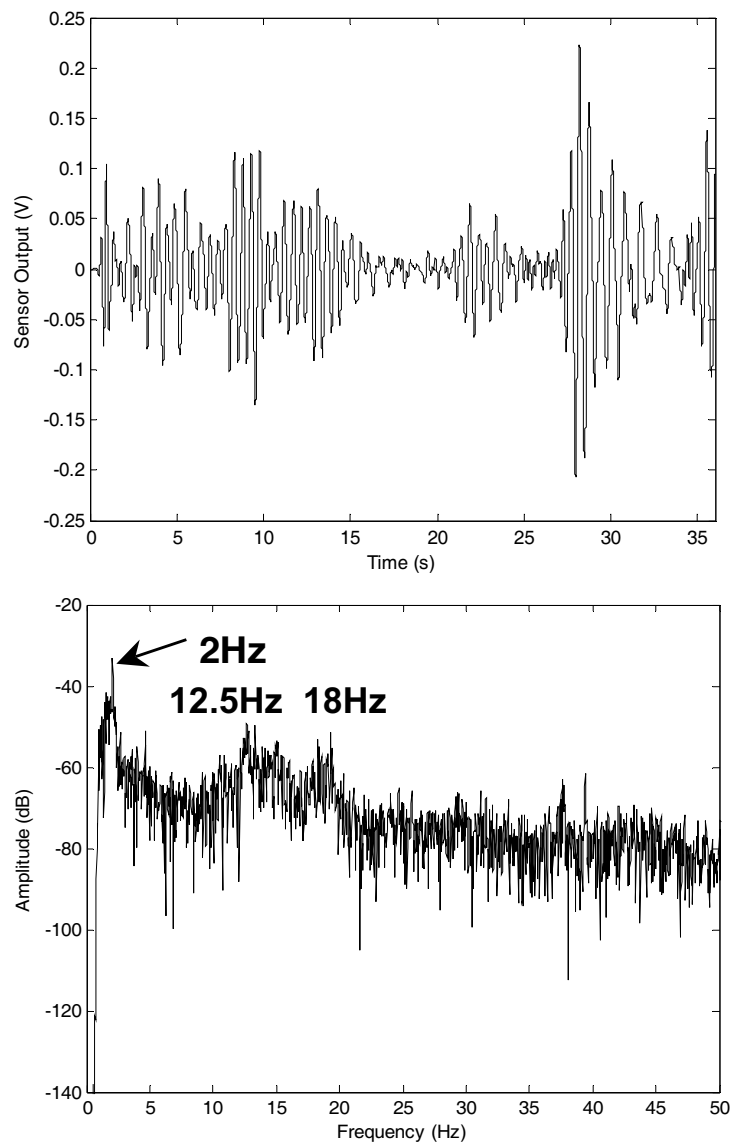


Fig. 13. Field test of traffic impact monitoring with 5 cars or trucks passing: (a) Time trace of the signal around 2 Hz, after 1 Hz-5 Hz bandpass filter; (b) Power spectrum up to 50Hz of the raw data after 1 Hz highpass filter.

The dynamic data was collected when cars and trucks were passing on the concrete slabs reinforced by FRP bars, hence the birefringence of the optical fiber attached to them would be affected. The sampling rate of our sensor was set to be 1 kHz as the frequencies of interest should be fairly low. A bandpass filter (1 Hz - 5 Hz) was applied on one set of the raw data to retrieve the signal around 2 Hz as plotted in Fig. 13(a) within 36 seconds. During this time

period, five cars and trucks passing on the two slabs were observed visually. Each vehicle represents one oscillation profile. In the first 15 seconds, it seems two or more impact events overlapping each other, as the damping time of the slab is much longer than the spacing time between cars. The maximum amplitude is at the 28th second, corresponding to a loaded truck passing by, and the damping time is for 6 seconds till the next impact event occurs. The weight of the car may be identified by its damping time; if the calibration of the car weight and decay time is characterized. Fig. 13(b) represents a typical power spectrum of the testing signal from 50 m sensing with the main frequency components below 20 Hz. This matches the previous research on dynamic testing of highway bridge using traffic loads (Bao et al., 2008). The first peak locates at 2 Hz, about 18 dB higher than the second peak at 12.5 Hz, and the third peak at 18 Hz. These three frequencies should correspond to the natural frequencies of the whole test slabs' structure. Apparently the frequency and damping time of the concrete slab can be determined by the proposed method.

7. Water wave frequency detection

Underwater acoustic sensing is an area in which fiber optic sensors have great advantages due to the possibility of multiplexing and distributed techniques existing in fiber communication and fiber sensor systems. Using the state of polarization (SOP) change in optical fiber under water one can measure the power spectrum of the oscillatory water currents due to water movement (Zhang et al., 2008b).

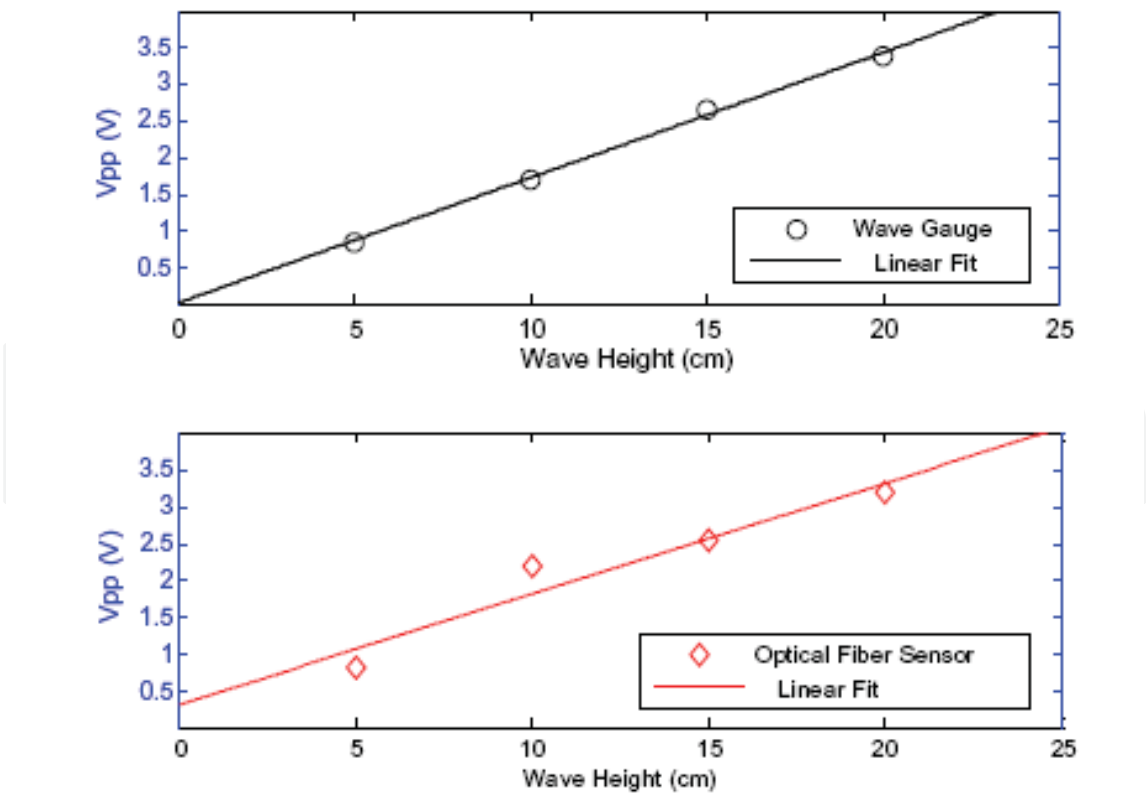


Fig. 14. Linearity of the (a) wave gauge and (b) optical fiber sensor.

In the experiment, the fiber has been laid across a section of wave flume, which is essentially a long water channel equipped with a wave generator at one end and a wave absorbing device at the other end; hence the fiber serves as a point sensor acting as a wave gauge. The fiber sensor is capable of detecting water wave frequencies accurately for all types of wave generated by the flume. With the optimum sag of fiber, the output response of the optical fiber sensor is linear within $0.7 \text{ m} \pm 0.2 \text{ m}$ wave level. Fig. 14 is the wave measurement by the wave gauge and fiber sensor.

The sensor monitors the polarization state change induced intensity variation of the light when the sensing fiber is affected by the presence of the water wave. As a result, the sensing fiber should be fully submerged in the water and be able to be moved physically by the water wave for the frequency range of 1-10 Hz, although the vibration sensor can have a KHz response signal. The sensor is capable of providing accurate frequency distributions for both regular waves and irregular waves, confirmed by a conventional wave gauge.

8. Spectral analysis of POTDR for intrusion sensing

Up to now, distributed optical fiber sensors have been mainly studied for static measurements, i.e. no time-varying or slowly time-varying signals, such as, static strain or temperature. Dynamic measurements using the above techniques are difficult to achieve because of the large number of waveforms required to average out the polarization effect induced signal fluctuation or because of the large range of frequency scans that are needed in order to obtain a reasonable signal to noise ratio (SNR) and spatial resolution over a kilometer fiber length.

A frequency modulated source to realize distributed Brillouin sensor based on correlation of pump and probe in fiber is demonstrated for vibration measurement (Hotate & Ong, 2003]. However, each time only one sensing point is chosen by the correlation peak of pump and probe light, it is particularly suitable for material processing over a short fiber distance while it is not essentially a fully distributed sensor which should provide information for every point along the fiber under test simultaneously. A truly distributed vibration sensor has been demonstrated recently based on the spectrum density of POTDR system (Zhang & Bao, 2008b). This new sensor can detect a vibration frequency of 5 KHz over 1 km sensing length with 10 m spatial resolution.

POTDR was developed as the first fully distributed optical fiber measurement for static physical parameters in the earlier 80's (Rogers, 1981) and then adopted as a diagnostic tool in optical communication systems to identify high polarization mode dispersion (PMD) fiber sections (Gisin et al., 1999). In conventional POTDR, the SOP is measured with 4 polarization controllers so that the rotation angle of SOP can be measured in every location to recover the PMD or strain, this process takes minutes, as a result, it can only be used for static measurement. To realize dynamic measurement with ms time scale, only one polarizer is sufficient to identify dynamic events, through which the birefringence change along the fiber could be detected; the setup is shown in Fig. 15. Moreover, with a novel fast Fourier transform (FFT) spectrum analysis, multiple simultaneous events with different vibration frequencies or even with the same frequencies are able to be accurately located. The spectral density function of location change is equivalent to many variable narrowband filters with bandwidth of $< 1\text{Hz}$ to improve the SNR of multiple events detection, which allows the disturbance to be detected simultaneously at any location along the sensing fiber.

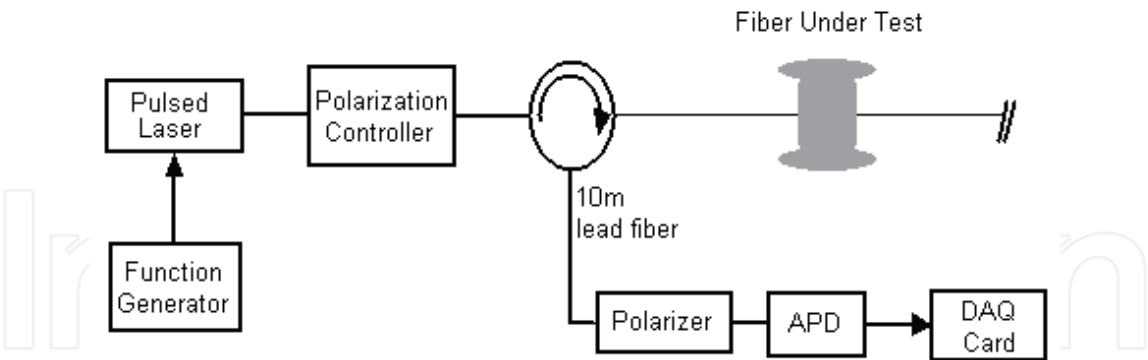


Fig. 15. Experimental setup of POTDR system

Data processing for the POTDR is done using four steps: in step (1) a large number of POTDR curves are acquired, step (2) at a particular position the time domain plot can be acquired from multiple POTDR curves, step (3) the FFT can be performed at that position using the time domain information and step (4) by performing steps (2) and (3) at all points along the fiber the magnitude of a certain frequency can be plotted as a function of distance. The post-signal processing is shown in Fig. 16. Step (1) to (3), is employed here by taking an average every 100 POTDR curves in step (2). Considering a 10 kHz repetition rate of the pulsed light, the effective sampling rate becomes 100 Hz, which has set the limitation for impact wave detection. Fig. 17(a) plots the FFT spectrum of 1.5 seconds time domain data at 550 m with a peak at 22 Hz when the PZT is driven by 5 Vpp, 22 Hz square wave. Benefited to its high sensitivity, this POTDR system makes it possible to measure higher frequency disturbance without any averaging in step (2). Hence, the maximum detectable frequency is 5 kHz using a 10 kHz sampling rate. In Fig. 17(b) when the driven frequency of the piezo is set to 4234 Hz, this peak frequency is clearly shown in the FFT spectrum at 550 m.

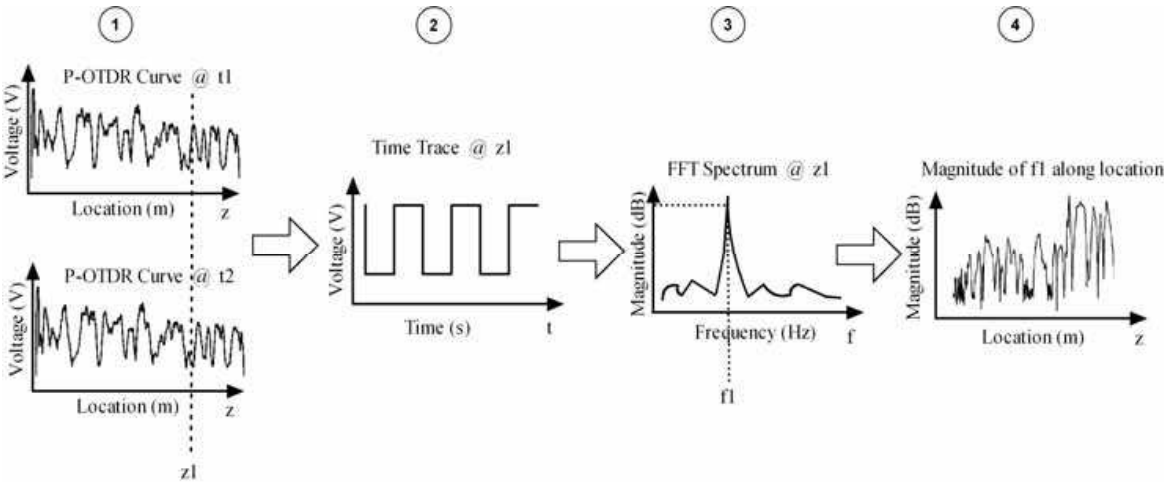


Fig. 16. The data processing of the spectrum density of POTDR

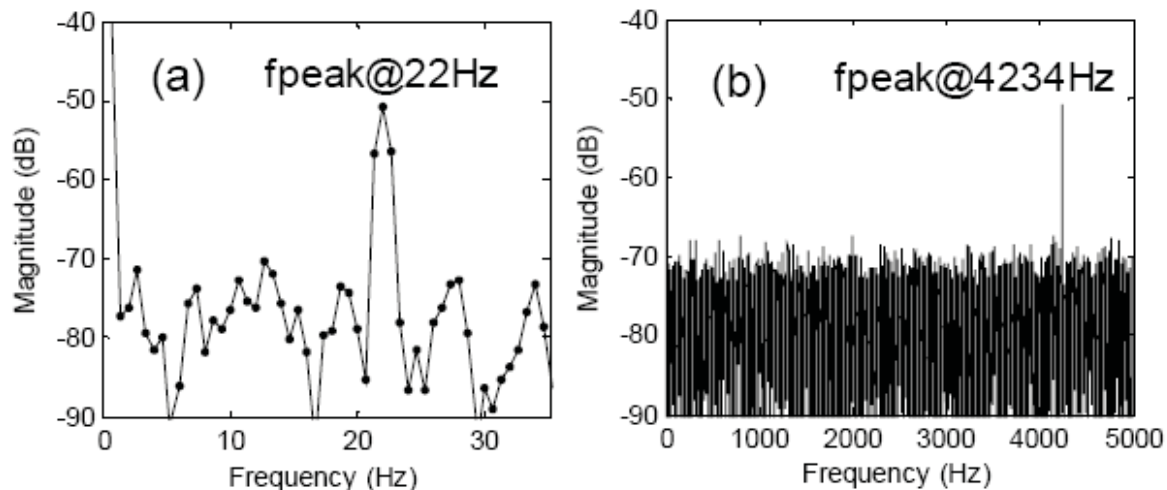


Fig. 17. Piezo fiber stretcher driven by 5 Vpp square wave, FFT spectrum of time trace signal at 550 m of (a) 22 Hz driven signal; (b) 4234 Hz driven signal

The present sensing uses post-signal processing, with the introduction of a micro-processor there would be a significant reduction of the signal processing time without going through computer for digitization and programming timing, which makes the current system response in the ms time frame, as the FFT signal processing and averaging can be conducted by electronic circuits directly. This new technology could in a cost-effective manner provide intrusion sensing for perimeter security at various places or structure health monitoring for large structures, such as bridges, highway pavements, pipeline leakage, etc. with low fault rate due to the multiple frequency components discrimination at < 1 Hz narrow band.

9. Conclusion

Monitoring of health is not a new idea and it is literally practiced by physicians using a knowledge base, tools, methods, and systems for diagnosis and then prognosis of one's state of health. Some of these tools were specifically developed for the practice of medicine and in a similar fashion this occurred in the current chapters.

The ability to accurately and efficiently monitor the long-term performance of engineering structures is an extremely valuable one. The potential benefits of structural monitoring includes reducing lifetime maintenance costs, improved safety and the ability to confidently use more efficient designs and advanced materials.

Today, a new and interdisciplinary area of structural health monitoring is likewise needed in order to address the structural, economic, and safety needs of the 21st century society and beyond. As with other industries, civil engineering must also undergo such a catharsis for a similar industry development.

In this Chapter we focused on fiber sensors using birefringence properties which have the fastest response to dynamic changes, using this idea combined with nonlinear effects we have demonstrated point and distributed sensors for dynamic monitoring in structures, communication fibers and security applications.

10. References

- Allen, C.; Kondamuri, P.; Richards, D. & Hague, D. (2003). Measured temporal and spectral PMD characteristics and their implications for network-level mitigation approaches. *J. Lightwave Technol.*, Vol. 21, No. 1, (January 2003) 79–86, doi:10.1109/JLT.2003.808634
- Bao, X.; W. Li, W.; Zhang, C.; Eisa, M.; El-Gamal S. & Benmokrane, B. (2008). Monitoring the distributed impact wave on concrete slab due to the traffics based on polarization dependence on the stimulated Brillouin scattering. *Smart Mater. Structures*, Vol. 17, No. 1, (November 2008) 1-5, doi:10.1016/j.engstruct.2004.05.018
- Barnoski, J. K. & Jensen, S. M. (1976). Fiber waveguides: A novel technique for investigation attenuation characteristics. *Appl. Opt.*, Vol. 15, No. 9, (Sept. 1976) 2112-2115
- Boyd, R. W. (2003). *Nonlinear Optics, Second Edition*, Academic Press, ISBN: 0-12-121682-9, San Diego
- Brosseau, C. (1998). *Fundamentals of Polarized Light: A Statistical Optical Approach*, Wiley Inter-Science, ISBN: 978-0-471-14302-4, New York
- Cameron, J.; Chen, L.; Bao, X. & Stears, J. (1998). Time evolution of polarization mode dispersion in optical fibers. *Photon. Technol. Lett.*, Vol. 10, No. 9, (September 1998) 1265–1267, ISSN: 1041-1135
- Chen, L.; Zhang, Z. & Bao, X. (2007). Combined PMD-PDL effects on BERs in simplified optical systems: an analytical approach. *Opt. Express*, Vol. 15, No. 5, (March 2007) 2106-2119, doi:10.1364/OE.15.002106
- Gisin, N.; Gisin, B.; der Weid, J. P. V. & Passy, R. (1996). How accurately can one measure a Statistical Quantity like Polarization-Mode Dispersion?. *Photon. Technol. Lett.*, Vol. 8, No. 12, (December 1996) 1671–1673, ISSN: 1041-1135
- Gordon, J. P. & Kogelnik, H. (2000). PMD fundamentals: polarization mode dispersion in optical fibers. *Proc. Nat. Acad. Sci.*, Vol. 97, No. 9, (April 2000) 4541-4550, PMID: 10781059
- Hotate, K. & Ong, S. L. (2003). Distributed dynamic strain measurement using a correlation-based Brillouin sensing system. *IEEE Photon. Technol. Lett.*, Vol. 15, No. 2, (February 2003) 272–274, ISSN: 1041-1135
- Huttner, B.; Gisin, B. & Gisin, N. (1999). Distributed PMD measurement with a polarization-OTDR in optical fibers. *J. Lightwave Technol.* Vol. 17, No. 10, (October 1999) 1843-1848, ISSN: 0733-8724
- Huttner, B.; Geiser, C. & Gisin, N. (2000). Polarization-induced distortion in optical fiber networks with polarization-mode dispersion and polarization-dependent losses. *IEEE J. Select. Topics Quantum Electron.*, Vol. 6, No. 2, (March/April 2000) 317-329, ISSN: 1077-260X
- Karlsson, M.; Brentel, J. & Andrekson, P. (2000). Long-term measurement of PMD and polarization drift in installed fibers. *J. Lightw. Technol.*, Vol. 18, No. 7, (July 2000) 941–951, ISSN: 0733-8724
- Krispin, H.; Fuchs, S. & Hagedorn, P. (2007). Optimization of the efficiency of aeolian vibration dampers, *Proceeding of Power Engineering Society Conference and Exposition in Africa*, South Africa, pp 1-3, ISBN: 978-1-4244-1477-2, July 2007, IEEE PowerAfrica '07, Johannesburg

- Landau, L. & Lifchitz, E. M. (1981). *Electrodynamics of Continuous Media* (J. B. Sykes & J. S. Bell, Trans.), Pergamon Press, ISBN: 0080091059, Oxford (Original work published 1969)
- Leeson, J.; Bao X.; Côté, A. (2009). Polarization Dynamics in Optical Ground Wire (OPGW) Network. *Appl. Opt.*, Vol. 48, No. 14, (May 2009) 2214-2219, doi:10.1364/AO.48.002214
- Measures, R. M. (2001). *Structural Monitoring with Fibre Optics Technology*, Academic Press, ISBN: 0-12-487430-4, London
- Rogers, A. J. (1981). Polarization-optical time domain reflectometry: A technique for the measurement of field distributions. *Appl. Opt.*, Vol. 20, No. 6, (March 1981) 1060-1074, ISSN: 0003-6935
- Snoody, J. (2008). *Study on Brillouin Scattering in Optical Fibers with Emphasis on Sensing*. Unpublished master's thesis, University of Ottawa, Ottawa, Canada
- Waddy, D.; Lu, P.; Chen, L. & Bao, X. (2001). Fast state of polarization changes in aerial fiber under different climatic conditions. *Photon. Technol. Lett.*, Vol. 13, No. 9, (September 2001) 1035-1037, ISSN: 1041-1135
- Waddy, D. S.; Chen, L. & Bao, X. (2005). Polarization effects in aerial fibers. *Opt. Fiber Technol.*, Vol. 11, No. 1, (October 2005) 1-19, doi:10.1016/j.yofte.2004.07.002
- Wuttke, J.; Krummrich, P. & Rosch, J. (2003). Polarization oscillations in aerial fiber caused by wind and power-line current. *Photon. Technol. Lett.*, Vol. 15, No. 6, (June 2003) 882-884, ISSN: 1041-1135
- Zhang, Z.; Bao, X.; Yu, Q. & Chen, L. (2006). Fast states of polarization and PMD drift in submarine fibres. *Photon. Technol. Lett.*, Vol. 18, No. 9, (May 2006) 1034-1036, ISSN: 1041-1135
- Zhang, Z.; Bao, X.; Yu, Q. & Chen, L. (2007). Time evolution of PMD due to the tides and sun radiation on submarine fibers. *Opt. Fiber Technol.*, Vol. 13, No. 1, (January 2007) 62-66, doi:10.1016/j.yofte.2006.07.003
- Zhang, Z. & Bao, X. (2008a). Continuous and damped vibration detection based on fiber diversity detection sensor by rayleigh backscattering. *J. Lightwave Technol.*, Vol. 26, No. 7, (April 2008) 852-838, ISSN: 0733-8724
- Zhang, Z. & Bao, X. (2008b). Distributed optical fiber vibration sensor based on spectrum analysis of polarization-OTDR system. *Opt. Express*, Vol. 16, No. 14, (July 2008) 10240-10247, doi:10.1364/OE.16.010240
- Zhang, Z.; LeBlanc, S.; Bao X. (2008a). Concrete pavement vibration monitoring due to the car passing using optical fiber sensor, *Proceedings of the 19th International Conference on Optical Fibre Sensors (OFS-19)*, pp.1-5, ISBN: 9780819472045, Australia, June 2008, SPIE, Perth
- Zhang Z.; Bao X.; Rennie C. D.; Nistor I. & Cornett A. (2008b). Water wave frequency detection by optical fiber sensor. *Opt. Communication*, Vol. 281, No. 24, (December 2008) 6011-6015, ISSN: 0030-4018



Optical Fiber New Developments

Edited by Christophe Lethien

ISBN 978-953-7619-50-3

Hard cover, 586 pages

Publisher InTech

Published online 01, December, 2009

Published in print edition December, 2009

The optical fibre technology is one of the hop topics developed in the beginning of the 21th century and could substantially benefit applications dealing with lighting, sensing and communication systems. Many improvements have been made in the past years to reduce the fibre attenuation and to improve the fibre performance. Nowadays, new applications have been developed over the scientific community and this book fits this paradigm. It summarizes the current status of know-how in optical fibre applications and represents a further source of information dealing with two main topics: the development of fibre optics sensors, and the application of optical fibre for telecommunication systems.

How to reference

In order to correctly reference this scholarly work, feel free to copy and paste the following:

Xiaoyi Bao, Jesse Leeson, Jeff Snoddy and Liang Chen (2009). Fiber Sensor Applications in Dynamic Monitoring of Structures, Boundary Intrusion, Submarine and Optical Ground Wire Fibers, Optical Fiber New Developments, Christophe Lethien (Ed.), ISBN: 978-953-7619-50-3, InTech, Available from: <http://www.intechopen.com/books/optical-fiber-new-developments/fiber-sensor-applications-in-dynamic-monitoring-of-structures-boundary-intrusion-submarine-and-optic>

INTECH
open science | open minds

InTech Europe

University Campus STeP Ri
Slavka Krautzeka 83/A
51000 Rijeka, Croatia
Phone: +385 (51) 770 447
Fax: +385 (51) 686 166
www.intechopen.com

InTech China

Unit 405, Office Block, Hotel Equatorial Shanghai
No.65, Yan An Road (West), Shanghai, 200040, China
中国上海市延安西路65号上海国际贵都大饭店办公楼405单元
Phone: +86-21-62489820
Fax: +86-21-62489821

© 2009 The Author(s). Licensee IntechOpen. This chapter is distributed under the terms of the [Creative Commons Attribution-NonCommercial-ShareAlike-3.0 License](https://creativecommons.org/licenses/by-nc-sa/3.0/), which permits use, distribution and reproduction for non-commercial purposes, provided the original is properly cited and derivative works building on this content are distributed under the same license.

IntechOpen

IntechOpen